ACS OMEGA

http://pubs.acs.org/journal/acsodf

Article

Structure and Optical Properties of Opal Films Made by an Out-of-Plane Electric Field-Assisted Capillary Deposition Method

Mulda Muldarisnur* and Frank Marlow

Cite This: *ACS Omega* 2022, 7, 8084−8090

Read Online

ACCESS | Metrics & More | Article Recommendations | Supporting Information

ABSTRACT: Self-assembled opals that are considered as a promising candidate for three-dimensional photonic crystals often suffer from the existence of internal defects. Defects influence optical properties and limit the applicability of opal films. Directed assembly using external fields may offer a certain degree of tunability in the opal formation process. We investigate the effect of an out-of-plane electric field on the formation and optical properties of opal films deposited using the capillary deposition method. The application of an electric field of intermediate strength (20−30 V/cm) can improve opal quality. The quality of opal films was found to depend on the polarity of the bottom substrate resulting from the beneficial influence of an asymmetry between the growths and the interplay with gravity. The negatively charged bottom substrate results in slightly better opal quality. This finding shows the potential of electric fields to tune opal formation in order to reduce the defect content.

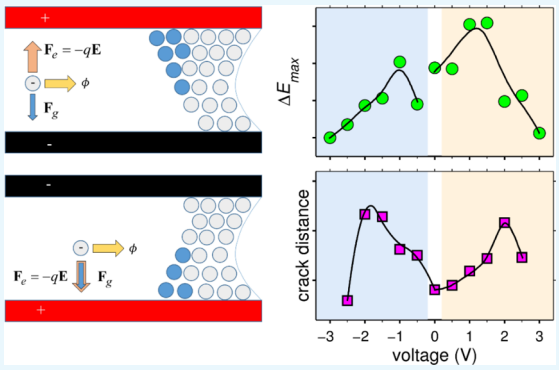

1. INTRODUCTION

Self-assembly of colloidal particles is a versatile and low-cost approach for fabrication of three-dimensional periodic structures called photonic crystals. Polychromatic electromagnetic waves propagate freely inside photonic crystals because of coherent cancelation of scattering effects except for those satisfying Bragg's law.[1] Interference of reflected waves at each internal interface results in optical band gaps where light propagation is forbidden. The existence of optical band gaps in photonic crystals allows controlling light−matter interactions at the nanoscale level. Furthermore, many applications of photonic crystals have been reported, for example, in waveguides,[2] reflectors,[3] beam splitters,[4] lasers,[5] sensors,[6] and many others.

Self-assembly utilizes natural tendency of monodisperse colloidal particles to form ordered close-packed arrangements known as colloidal crystals or artificial opals. Self-assembly is applicable for a large range of particle sizes and, therefore, can be used to tune the position of the band gap to match the intended applications. This is a big advantage over top-down approaches such as lithographic techniques that face difficulties in realizing three-dimensional photonic crystals with an optical band gap in the visible range. Many self-assembly methods have been proposed, for example, sedimentation,[7] horizontal deposition,[8] vertical deposition,[9] confinement cell deposition,[10] and capillary deposition.[11] In the sedimentation method, gravity drives settlement of particles onto a substrate that starts to crystallize after reaching a certain filling fraction. Natural sedimentation is very straightforward, but its use is limited only for particles that do not sediment too slow or too fast. In addition, the morphology, thickness, and crystallinity of obtained opals are difficult to control. The other above-mentioned self-assembly methods employ capillary and drag forces due to solvent evaporation to assemble particles on a substrate. The differences are in the details of the particle-ordering mechanism due to different boundary conditions. It is well-accepted that capillary and evaporation-based methods result in better opal quality than the sedimentation method. However, it also results in opals containing unintended internal defects like vacancies, dislocations, domains, and cracks.[12] The exact amount and types of internal defects in opals depend on the details of deposition and suspension conditions. Defects break the crystal symmetry and form defect states that in the case of a high concentration may lead to the closing of the optical band gap.[13,14] The improved controllability of the self-assembly process has long been desired by researchers.

External fields can be applied to attain a better-controlled opal deposition process. Besides optical and magnetic fields, electric fields are of a particular interest because they can be used for almost all types of colloidal particles in suspension due to the possession of surface charges. Surface charges are formed due to dissociation of a surface functional group or

Received: December 31, 2021
Accepted: February 9, 2022
Published: February 24, 2022

https://doi.org/10.1021/acsomega.1c07391
ACS Omega 2022, 7, 8084−8090

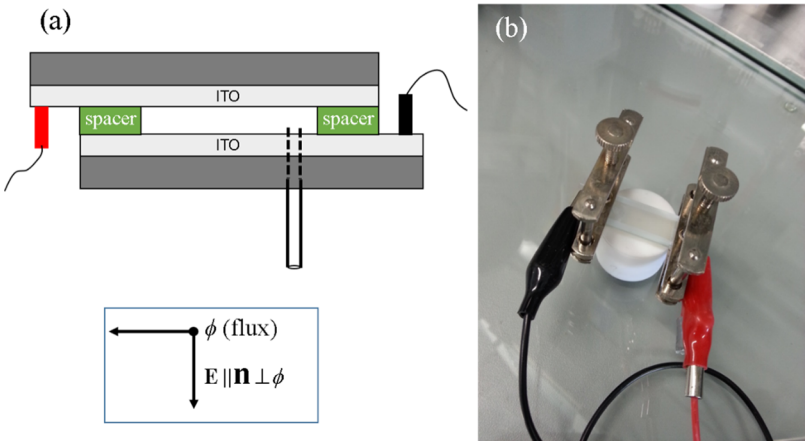

Figure 1. Experimental setup for opal deposition using the electric field-assisted CDM. (a) Cross section of a planar capillary cell and direction of the electric field with respect to the normal of the opal substrate **n** and suspension flux direction ϕ (inset) and (b) camera image of opal deposition. Opal deposition along open edges of the cell is visible in Figure (b).

adsorption of a specific ion from solution. The electro neutrality of suspensions requires the surface charges to be balanced by an equal number of distributed opposite charges around particles. The interaction between a particle and the others or external electric fields is dictated by the charge distribution.

Electric fields have been used for rapid and low-cost particle assembly on various surfaces with complicated shapes in coating and microelectronic industries.[15,16] In this process, charged particles are deposited on an electrode of opposite polarity by applying a DC voltage. An electric field was used to adjust the sedimentation rate that is too slow for small particles and too fast for big ones and therefore improves the crystallinity of the resulting opals.[17,18] The authors reported an improved ordering quality and larger domain size. Theoretical and experimental work on electrophoretic sedimentation methods showed that there is a crystallinity gradient along the growth direction, well-ordered near the substrate but deteriorated away from the substrate.[19] Electric fields have also been applied for opal deposition using the vertical deposition method.[20−22] The authors showed that the electric field enables fast deposition of thick opal films with an improved particle ordering and larger domain size. However, despite some improvements, thickness variations along the growth direction and random hexagonal close packing were still observed.

To the best of our knowledge, there was no previous study on opal deposition under the influence of an electric field oriented perpendicular to the crystal growth front. It is interesting to know whether the coupling of an electric field with the flow of charged particles may lead to a change of opal film quality. The capillary deposition method (CDM) is an excellent option for this kind of study. Compared to other methods, the CDM offers additional advantages that are as follows: (1) well-defined growth and drying fronts, (2) predetermined opal thickness independent of deposition or suspension parameters, (3) no thickness gradient, (4) applicable for a large range of particle size, and (5) separated deposition and drying processes. Therefore, in this work, we report an application of an electric field to influence opal formation. We found that electric fields perpendicular to the growing opal film indeed have a significant influence on the properties of the resulting opals.

2. EXPERIMENTAL DETAILS

2.1. Construction of the Deposition Cell. In the CDM, an opal film is deposited inside a planar capillary cell constructed by sandwiching two glass slides separated by two thin polymer spacers. In this work, indium tin oxide (ITO)-coated glass slides (15 mm × 42 mm) were used as substrates. Polymer spacers with a thickness of 50 μm (Pütz-Folien GmbH) were used to define the thickness of the resulting opal films. A hole with 1 mm diameter was drilled at a distance of 15 mm from the upper glass slide edge (see Figure 2) to mount a capillary tube. The tube was used to transport the colloidal suspension from a Teflon container into the planar capillary cell. Before cell construction, the ITO-coated glass slides were cleaned using Labosol (Neolab GmbH) following steps that have been published before[23] but without ultrasonication and mechanical cleaning. For cell construction, freshly cleaned glass slides were dried with a nitrogen flow. A capillary tube (18 mm long) was fixed into the drilled hole and then glued using epoxy resin. Two polymer spacers (each about 2 mm × 15 mm) were placed onto the second glass slide by using tweezers. After the glue dried, the glass slides were sandwiched and then connected tightly using Parafilm.

A 0.5 wt % suspension of polystyrene (PS) was obtained by diluting a 10 wt % suspension (Microparticles GmbH) with milli-Q water without prior treatment. Vibration from an ultrasonic bath (20 min) was used to ensure suspension homogeneity. The diameter of PS particles was 320 ± 8 nm. The particles are negatively charged arising from sulphate functionalization counter balanced with K^+ ions. Negative charge remains on the PS surface, while K^+ ions are released into the suspending medium. The suspensions used in this work have high zeta potentials (50−70 mV, manufacturer information) leading to very good stability.

2.2. Opal Deposition. In this version of the CDM, two metallic clamps were used as sample holders during the deposition process. The clamps additionally maintain the stability and the planarity of the planar capillary cell. Opal deposition started shortly after the tube of the planar capillary cell was immersed into the colloidal suspension. The capillary force inside the tube lifts the suspension up from the container into the planar capillary cell. The capillary force and solvent evaporation at the two open edges spread the suspension inside the planar cell and pull colloidal particles toward the

https://doi.org/10.1021/acsomega.1c07391
ACS Omega 2022, 7, 8084−8090

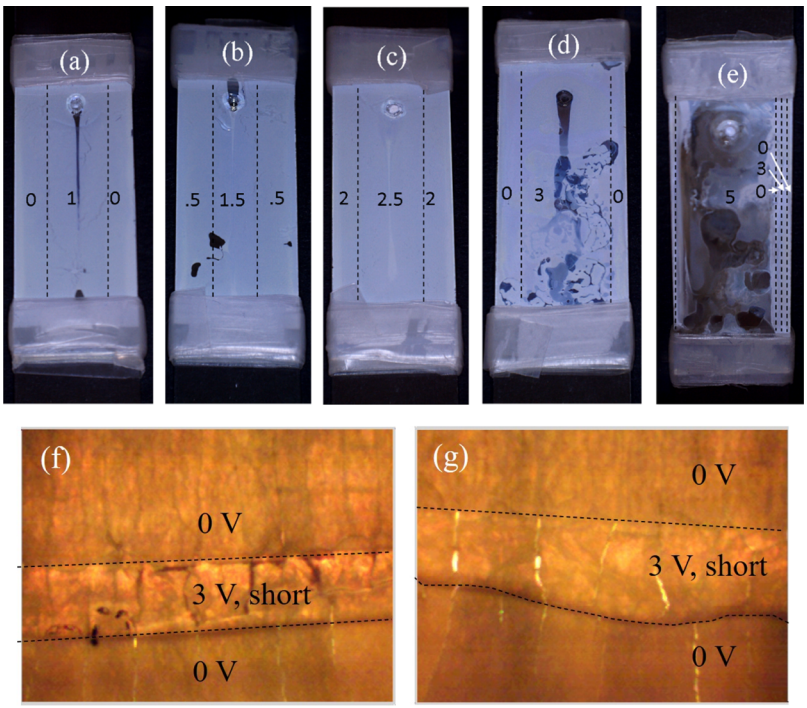

Figure 2. (a–e) Camera images and (f,g) optical microscope images of samples deposited at different voltages. The applied voltage is noted in the images.

menisci. Particle aggregation along the menisci forms many crystal nuclei that grow together toward the center of the capillary cell. The growth front is parallel to open edges before being curved near the spacers after the crystal fills more than a half of the capillary cell. The balance between continuous suspension supply and solvent evaporation results in a stable opal growth. All opal samples were deposited in a room with well-regulated temperature (21 ± 1 °C) and relative humidity (42 ± 1.5%).

An electric field inside the planar capillary cell was generated between the two (ITO)-coated glass slides by a power supply (BaseTech BT-153). The terminals were connected to the ITO-coated glass slides as shown in Figure 1 using crocodile clips. The direction of the electric field was varied by exchanging the polarity of the ITO-coated glass slides. The output voltage of the power supply was varied between 0 and 5 V with steps of 0.5 V. These voltages correspond to an electric field strength of 0–100 V/cm. When the capillary cell was filled completely with the wet opal, the cell was detached from the suspension to initiate the drying process. The drying process took place under room conditions similar to deposition. The voltage was switched off during the drying process. The progress of opal deposition and drying processes was followed using a camera.

2.3. Structural and Optical Characterization. Visual observation is a first direct mean of evaluating opal quality. Good opals show brilliant and homogeneous opalescence over the whole area of the sample. At a smaller scale, the structure of the opal films between tens and hundreds of micrometers was investigated by using optical microscopes. In this range, domains and cracks appear as characteristics of the opals. Observation was performed using a Leitz Orthoplan optical microscope. Images were captured in the transmission mode at an objective magnification of 16× with the illumination from a halogen or a xenon lamp and recorded by using a microscope camera (MA 888, AmScope). The uncertainty of the measured crack distance at this magnification is about 4 μm. Particle ordering at a sub-micrometer scale was probed using a scanning electron microscopy (SEM) microscope (Hitachi S-3500N) operated at 10–20 keV. For this purpose, the capillary cell must be opened, and then, a 10 nm-thick gold layer was deposited on the opal sample to prevent charge accumulation on particle surfaces. Accumulated charges repel and deviate the path of incoming electrons and cause image distortion. A C-mount microscope camera was used to capture the sample image every minute during opal formation. The stack of images was converted into a movie (AVI format, seven frames per second) using Image-J software.

The optical band gap of opals is manifested in the transmission dip at a certain range of wavelength. A Cary 5G UV–vis spectrometer (Varian GmbH) operated in a double-beam mode was used for transmission measurements. The UV and Vis–NIR light of the spectrometer is provided by deuterium and quartz–iodine incandescence lamps, respectively. The transmitted light through the opal sample was detected using a photomultiplier (for UV–Vis light) and a PbS photocell (for NIR light). All measurements were carried out at normal incidence (light perpendicular to the opal film).

3. RESULTS AND DISCUSSION

3.1. Structure of Opal Films. At low electric field strength, there is no significant macroscopic difference in opal formation when deposited on ITO-coated or normal glass slides. Wet opal films start to form along the open edges where the solvent evaporates. The evaporation drags particles into the growth front that is oriented parallel to the open edges or perpendicular to the suspension flux direction. Wet opals are composed by a non-close-packed particle arrangement due to repulsive interactions among particles. The detailed mechanism of wet opal formation from suspension on CDM-made

https://doi.org/10.1021/acsomega.1c07391
ACS Omega 2022, 7, 8084–8090

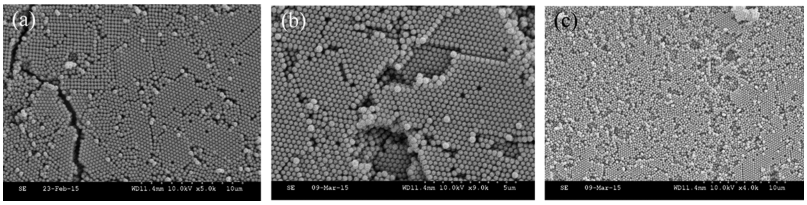

Figure 3. SEM images of opal samples deposited at electric fields of (a) 0, (b) 30, and (c) 60 V/cm.

opals had been discussed before.[24] Contrary to common belief, the drying process is not simply solvent removal; instead, it involves particle reorganization and compaction.[25] The result is a dry thin opal film. Not only the general appearance of the deposition process but also its speed was not significantly affected by the applied electric field.

A substantial difference was observed at higher electric field strength. Opal formation is hindered by gas formation when the applied electric field is above 60 V/cm (see the Supporting Information). Once deposition was disturbed, no deposition occurred again even when the applied field was removed.

Some images of opal films deposited using the CDM under the influence of the electric field are shown in Figure 2. Nearly homogeneous films were obtained at lower voltage (Figure 2a−c). These opal samples are homogeneous. The empty areas in Figure (b) are due to partly unclean substrates. Disordered opals were obtained when deposited at voltage ≥ 3 V (electric field 60 V/cm). No opals can be deposited when the applied field is 100 V/cm (Figure 2e). The dashed lines were added to indicate the border between two parts of opals deposited at different voltages.

The clear boundary on opal films deposited at different voltages indicates significant influence of the electric field on particle ordering (Figure 2f,g). Different homogeneity and crack spacing are also visible. The opal deposited at 0 V/cm is obviously of different quality than that deposited at higher field strength. In this sample, the higher voltage was only applied for a short time leading to no significant gas generation by electrolysis.

Larger homogeneous opals were obtained only for applied electric fields lower than 60 V/cm. When the applied voltage was larger, the suspension remained opaque even after voltage was switched off. The electrolytic formation of hydrogen and oxygen at the substrates occurs at high voltage and causes the suspension to become opaque. Gas trapping inside the capillary cells prohibits formation of a homogeneous opal film. As a result, opaque and empty areas were formed. The decomposition of water-based suspensions at high electric fields has also been reported for opals deposited using sedimentation[17] and vertical deposition.[21,22]

SEM images of opal samples deposited at different electric fields are shown in Figure 3. The face-centered cubic (fcc) structure with the (111) plane showing a hexagonal particle arrangement is known for opals deposited on solid substrates. The tendency of particles to form the close-packed arrangement well aligned with the substrate is related to energy minimization. Opals deposited at 0 V/cm on ITO-coated glass slides also show hexagonal particle arrangement mostly, however, with visible rectangular arrangements [(100)-orientation] in some areas. Only hexagonal particle arrangements were found for opals deposited at 30 V/cm. Random particle arrangements in some parts of the sample were visible for opals deposited at 60 V/cm. Vacancies on the surface of opals are likely formed during cell opening before taking the SEM images.

The good particle ordering for opal films deposited at 30 V/cm indicates that there is an optimum electric field strength for particle ordering and attachment on the substrate. Charged particles in a suspension undergo electrophoretic migration due to the interaction of the electric double layer with the electric field. The electrophoretic mobility of charged particles depends on the suspension concentration, electric field, and zeta potential.[16] During deposition, the electric field and the gravity are in the same direction, and negatively charged PS particles are attracted by the positive (upper) substrate and repulsed by the negative (bottom) substrate. A large electric field causes rapid attachment of colloidal particles on the upper substrate and inhibition of particles to fill the volume nearby the bottom substrate. Therefore, the crystal formation starts at the upper substrate, and a competition of two crystal structures is avoided. It seems that the optimum electric field is about 30 V/cm. The high degree of ordering for opals deposited at 30 V/cm suggests that the arrival rate of particles at the growth front is low enough to give sufficient time for finding low-energy sites before the next particles inhibit further movement. Details on the packing mechanism need further investigation. Uniform films deposited at moderate electric field strength (25−100 V/cm) have been also reported for zirconia.[26]

3.2. Optical Properties. Ordering quality of opal films is manifested in the occurrence of Bragg peaks. Figure 4 shows extinction spectra of opal samples deposited with a negative bottom slide. The negatively charged bottom substrate can avoid fast aggregation and attachment because the colloidal particles possess negative charges. Spectra of opal films deposited at different voltages are obviously different. The height and the width of a Bragg peak depend in a non-

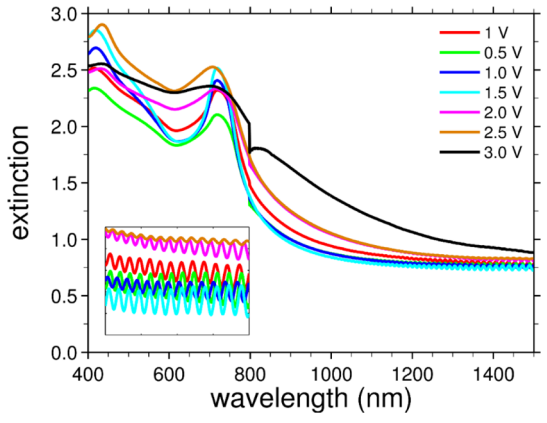

Figure 4. Extinction (−log T) spectra of CDM-made opals deposited at different field strengths. During deposition at positive field strength, the upper and bottom substrates were connected to the positive and negative terminals, respectively. Inset: Fabry−Perot oscillations.

https://doi.org/10.1021/acsomega.1c07391
ACS Omega 2022, 7, 8084−8090

monotonous manner on the applied electric field. The continuous background that decreases with wavelength[23] has a decreasing slope at high field strength. The background of the spectra of an opal deposited at 60 V/cm is much higher than that of the others. The position of the peak is, however, independent of the applied voltage.

The peak in the extinction spectra corresponds to the optical band gap originating from Bragg diffraction of the opal lattice. The center of the Bragg peak can be calculated using Bragg's law $\lambda_B = 2n_{eff}d_{hkl}\cos\theta_{hkl}$, where n_{eff}, d_{hkl}, and θ_{hkl} are the effective refractive index, the interplanar distance, and the angle between (hkl) direction and the incident light beam, respectively. The effective refractive index of the opal can be approximated by the volume-averaged refractive index of particles (n_p) and the medium (n_m), $n_{eff} = n_p f_p + (1 - f_p)n_m$. For fcc crystals like opals, $f_p = 0.74$ and the interplanar distance is $d_{hkl} = \sqrt{2}D(h^2 + k^2 + l^2)^{-1/2}$, where D is the diameter of the colloidal particles. For the normal incident angle of light, the main diffracting plane is (111), therefore $\theta_{111} = 0$. Inserting the refractive index of PS (1.59) and $n_m = 1$ for the surrounding medium (air), one obtains $n_{eff} = 1.44$, therefore $\lambda_{111} = 2.35D = 752 \pm 19$ nm that is in good agreement with the average measured value (740 nm). Small deviation in the measured position of Bragg is caused by the particle sintering during opal drying.[27]

The quality of the particle ordering is also visible by the Fabry−Perot oscillation at long wavelength. The oscillation indicates surface flatness and homogeneity for the 50 μm-thick (almost 200 layers) samples. The Fabry−Perot oscillations were reported for opals deposited using another method but for much thinner films.[14,28] The oscillation is not visible for the sample deposited at 60 V/cm. Fabry-Perot oscillations can also be used to calculate opal thickness. Film thickness satisfies $h = \lambda_i/(2n_{eff}(1 - \lambda_i/\lambda_{i+1}))$, where λ_i and λ_{i+1} are neighboring peaks with $\lambda_i < \lambda_{i+1}$. Substituting $n_{eff} = 1.44$, $\lambda_i = 1465$ nm, and $\lambda_{i+1} = 1480$ nm results in a thickness of 50.1 μm that is in good agreement with the thickness of spacers.

The maximum extinction of the opal samples is in the range of 2.0−2.5, that is, equivalent to a reflectance of more than 99%. The high reflectance indicates efficient inhibition of light from entering the photonic crystal and a low partial transmission mediated by defects. The measured reflectance is much higher than reported values in the literature. Reflectance values below 70% were reported for opals deposited using a sedimentation method,[7] vertical deposition method,[22,28] and horizontal deposition method.[8] Extinction is thickness-dependent; therefore, only spectra from samples above a critical thickness (13 layers)[29] were considered here.

For a better comparison between spectra of the opal samples, the spectral features were plotted in Figure 5. The spectra of samples with a positively charged bottom substrate (BP^+) were added for comparison. The graph shows that the quality of opal films is affected by the electric field applied during opal deposition. The height of Bragg peaks of opals deposited with a positive bottom substrate slightly differs from that of opals deposited with a negative bottom substrate (BP^-). The optimum voltage for BP^+ is 1 V (electric field 20 V/cm) while for BP^- is at 1.5 V (electric field 30 V/cm). The height of the Bragg peak in both cases significantly decreases when opals are deposited at 60 V/cm, with the decrease being much steeper for BP^+. The ΔE_{max} for BP^+ tends to be lower than that of BP^- for the same electric field strength. The

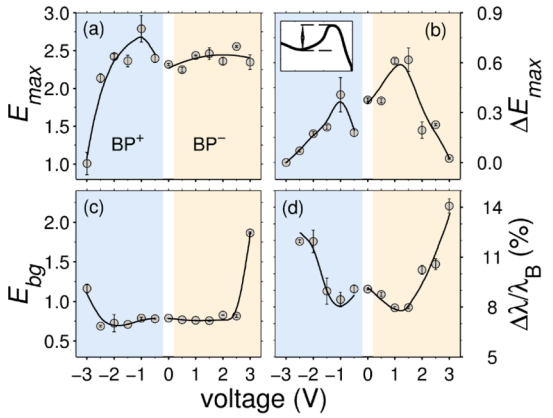

Figure 5. Spectral features of opal films for different applied voltages, (a) maximum extinction, (b) background-subtracted maximum extinction, (c) background at 1400 nm, and (d) normalized fwhm.

change of the background on the electric field has a similar trend for opals deposited with the positive (BP^+) and negative (BP^-) bottom substrate. Background increases suddenly when the electric field is above 60 V/cm. There exists a minimum peak width [normalized full width at half-maximum (fwhm)] for each substrate polarity. The Bragg peak broadens when the applied voltage is larger than or equal to 2 V (electric field 40 V/cm).

The maximum extinction shows a non-monotonous dependence on the applied electric field. It reaches a maximum for the applied field of 20−30 V/cm. The influence of the external electric field becomes more visible after subtracting the continuous background from the maximum extinction (ΔE_{max}). The ΔE_{max} has also the maximum when the applied field is 30 V/cm. The Bragg peak decreases at high applied voltage, and no Bragg peak is observed at 100 V/cm. The height of the Bragg peak depends on refractive index contrast between particles and medium and film thickness and crystallinity. The first two parameters are the same for all samples. Therefore, variation in Bragg peak height can only be caused by different crystallinity. The higher Bragg peak for samples deposited under the application of the electric field shows that the field of a certain range can improve the ordering. We ascribe this to a beneficial role of the field-induced symmetry breaking between the bottom and the top substrate. In fully symmetric systems, we have a competing growth of ordered domains on both substrates inducing a lot of domain boundaries. By application of the field, this effect is reduced, and larger domains are formed at one of the electrodes.

The slight dependence on the polarity of the bottom substrate implies an interplay with gravity. When substrates are connected to a power supply, upper and bottom substrates possess opposite charges. As a result, an electric field is generated inside the capillary cell. The electric field results in Coulomb forces in the charged colloidal particles. The screening effect reduces the net charge of the particles significantly. However, screening does not act homogeneously. Near to the substrates, the screening clouds are disturbed leading to a stronger attachment force in comparison to the transport force in the middle of the capillary. In contrast, the gravity acts homogenously. Therefore, both forces, the electric and the gravitational, do not replace each other completely. Their interplay allows the tuning of attachment forces in

https://doi.org/10.1021/acsomega.1c07391
ACS Omega 2022, 7, 8084−8090

comparison with transport forces. There are two scenarios: the electric field parallel or opposite to the gravitational force. When the bottom plate is negative, gravitation and electric forces working on colloidal particles are antiparallel, and the transport force is reduced or even overcompensated. When the bottom plate is positive, gravitation and electric forces are in the same direction. Therefore, a positive bottom substrate leads to rapid particle attachment and less time to find minimum energy sites especially on the bottom substrate. On the contrary, a negative bottom substrate results in repulsion on approaching particles so that the particles have more time to find minimum energy sites especially near the substrate. As a result, opal films with higher quality can be obtained.

The background of the spectra is nearly constant for applied fields below 50 V/cm, and then, it suddenly increases independently of substrate polarity. The background results from scattering by defects that can be described by Mie-like scattering.[23] The applied field also has a significant influence on the fwhm of the Bragg peak that also reflects the lattice disturbances. The fwhm decreases with the electric field, reaches its minimum, and then increases again as the background behaves. The electric field above 40 V/cm broadens the fwhm significantly. The bad opal quality when deposited at high field strength is also obvious from the microscope and SEM images.

3.3. Crack Distance. Soon after detachment of the planar capillary cell from the suspension container, the drying process started. The start of the drying process is indicated by an obvious change in the transparency of the opal films. In the initial stage of drying, opal films turn opaque due to particle rearrangement, refractive index contrast increase, and crack formation.[23,30] Cracks propagate from the open edges of the cell inward into the center of the planar capillary cell following the movement of the drying front. Cracks are formed due to unbalanced shrinkage of the opal films and substrate that builds internal stress when the solvent in the interstitial voids between particles evaporates. The cracks in CDM-made opals deposited under the influence of the electric field are nearly parallel to each other, similar to the crack alignment for normal CDM-made opals. The average distance between cracks is known to be thickness-dependent[15,31] due to the need to balance between the needed cleavage energy and the energy recovered from elastic relaxation in the vicinity of the crack.

Average crack distance of opal samples as a function of the applied voltage is shown in Figure 6. The crack distance of each sample was averaged over more than 30 measured cracks for a good statistic. The obtained crack distance is 110−155 μm, larger than the values in the literature for opals prepared using other methods.[13,28,32] The crack distance tends to increase with the applied voltage up to 2.0 V (electric field 40 V/cm) before it decreases significantly. Maximum crack distance is obtained at a voltage of 2 V independently of substrate polarity. At a voltage equal to or larger than 3 V, due to water decomposition, no homogeneous opal films were formed, while many empty and disordered areas were observed. This is the reason why the crack distance cannot be displayed at high voltage.

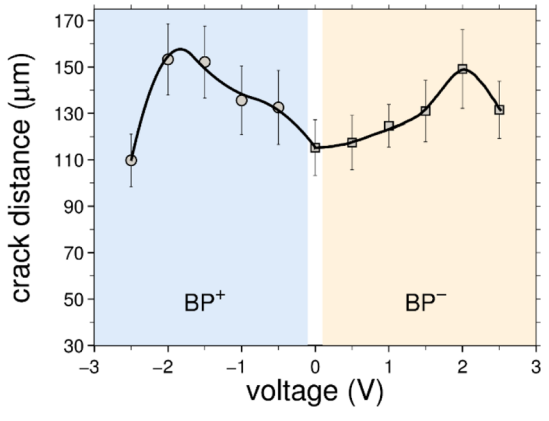

Figure 6. Average crack distance of thin opal films deposited using the electric field-assisted CDM as a function of the applied voltage.

The power supply was switched off during drying, while cracks are formed during this stage. The dependence of the average crack distance on a previously applied voltage indicates that the domain size is likely maintained during the later drying process. The electric field influences particle ordering and can enlarge the crystal domain size. The increase in domain size with the electric field had also been reported for opals deposited using the vertical deposition method.[33]

4. CONCLUSIONS

We have shown a significant influence of the electric field on the structure and optical properties of CDM-made opals. The influence is surprising on the first view because the electric field is perpendicular to the opal growth front. The electric field at intermediate strength leads to formation of high-quality opal films indicated by a sharp Bragg peak and a low background. The detailed mechanism of opal growth under the application of the electric field, however, needs further investigation.

We found that the electric field of a certain range results in better opal quality that shows the beneficial influence of an asymmetry between the growth at the bottom and at the top substrate. Optimum field strength for deposition using the CDM is 30 V/cm. A bottom substrate with negative polarity results in slightly better opal quality that is likely related to an interplay with gravity. Electric fields above 60 V/cm lead to disordered samples due to water decomposition on the surface of ITO substrates. The combination of a well-chosen electric field and the predetermined thickness of CDM-made opal films seems to us very promising for improved controlled opal deposition.

■ ASSOCIATED CONTENT

Supporting Information

The Supporting Information is available free of charge at https://pubs.acs.org/doi/10.1021/acsomega.1c07391.

Set of images taken one per minute during opal formation stacked to form a movie with seven frame per second and formation of an inhomogeneous wet opal film (AVI)

(AVI)

■ AUTHOR INFORMATION

Corresponding Author

Mulda Muldarisnur − *Department of Physics, Faculty of Mathematics and Natural Sciences, Universitas Andalas, Padang 25163, Indonesia;* orcid.org/0000-0002-0086-8753; Email: muldarisnur@sci.unand.ac.id, marlow@mpi-muelheim.mpg.de

https://doi.org/10.1021/acsomega.1c07391
ACS Omega 2022, 7, 8084−8090

Author

Frank Marlow − *Max-Planck-Institut für Kohlenforschung, Mülheim an der Ruhr 45470, Germany; CENIDE—Center for Nanointegration Duisburg-Essen, Duisburg 47057, Germany;* orcid.org/0000-0002-8539-8171

Complete contact information is available at: https://pubs.acs.org/10.1021/acsomega.1c07391

Notes

The authors declare no competing financial interest.

■ ACKNOWLEDGMENTS

The authors would like to thank Silvia Palm for SEM images and the Max Planck Society for funding the project. M.M. would like to thank the Ministry of Education and the Culture/National Research and Innovation Agency (no: 104/E4.1/AK.04.PT/2021) for funding.

■ REFERENCES

(1) Joannopoulos, J. D.; Johnson, S. G.; Winn, J. N.; Meade, R. D. *Photonic Crystals Molding the Flow of Light*, 2nd ed.; Princeton University Press: New Jersey, 2008; pp 1−286.

(2) Dutta, H. S.; Goyal, A. K.; Srivastava, V.; Pal, S. Coupling Light in Photonic Crystal Waveguides: A review. *Photonics Nanostructures: Fundam. Appl.* **2016**, *20*, 41−58.

(3) Curtin, B.; Biswas, R.; Dalal, V. Photonic Crystal Based Back Reflectors for Light Management and Enhanced Absorption in Amorphous Silicon Solar Cells. *Appl. Phys. Lett.* **2009**, *95*, 231102.

(4) Bayindir, M.; Temelkuran, B.; Ozbay, E. Photonic-crystal-based Beam Splitters. *Appl. Phys. Lett.* **2000**, *77*, 3902−3904.

(5) Kim, S.-H.; Kim, S.-H.; Jeong, W. C.; Yang, S.-M. Low-Threshold Lasing in 3D Dye-Doped Photonic Crystals Derived from Colloidal Self-Assemblies. *Chem. Mater.* **2009**, *21*, 4993−4999.

(6) Fathi, F.; Rashidi, M.-R.; Pakchin, P. S.; Ahmadi-Kandjani, S.; Nikniazi, A. Photonic crystal based biosensors: Emerging inverse opals for biomarker detection. *Talanta* **2021**, *221*, 121615.

(7) Mayoral, R.; Requena, J.; Moya, J. S.; López, C.; Cintas, A.; Miguez, H.; Meseguer, F.; Vázquez, L.; Holgado, M.; Blanco, Á. 3D Long-range ordering in ein SiO2submicrometer-sphere sintered superstructure. *Adv. Mater.* **1997**, *9*, 257−260.

(8) Müller, M.; Zentel, R.; Maka, T.; Romanov, S. G.; Torres, C. M. S. Dye-Containing Polymer Beads as Photonic Crystals. *Chem. Mater.* **2000**, *12*, 2508−2512.

(9) Jiang, P.; Bertone, J. F.; Hwang, K. S.; Colvin, V. L. Single-Crystal Colloidal Multilayers of Controlled Thickness. *Chem. Mater.* **1999**, *11*, 2132−2140.

(10) Yin, Y.; Lu, Y.; Gates, B.; Xia, Y. Template-Assisted Self-Assembly: A Practical Route to Complex Aggregates of Monodispersed Colloids with Well-Defined Sizes, Shapes, and Structures. *J. Am. Chem. Soc.* **2001**, *123*, 8718−8729.

(11) Li, H.-L.; Dong, W.; Bongard, H.-J.; Marlow, F. Improved Controllability of Opal Film Growth Using Capillaries for the Deposition Process. *J. Phys. Chem. B* **2005**, *109*, 9939−9945.

(12) Marlow, F.; Muldarisnur, M.; Sharifi, P.; Brinkmann, R.; Mendive, C. Opals: Status and Prospects. *Angew. Chem., Int. Ed.* **2009**, *48*, 6212−6233.

(13) Astratov, V. N.; Adawi, A. M.; Fricker, S.; Skolnick, M. S.; Whittaker, D. M.; Pusey, P. N. Interplay of Order and Disorder in the Optical Properties of Opal Photonic Crystals. *Phys. Rev. B: Condens. Matter Mater. Phys.* **2002**, *66*, 165215.

(14) Rengarajan, R.; Mittleman, D.; Rich, C.; Colvin, V. Effect of disorder on the optical properties of colloidal crystals. *Phys. Rev. E: Stat., Nonlinear, Soft Matter Phys.* **2005**, *71*, 016615.

(15) Van der Biest, O. O.; Vandeperre, L. J. Electrophoretic Deposition of Materials. *Annu. Rev. Mater. Sci.* **1999**, *29*, 327−352.

(16) Besra, L.; Liu, M. A review on fundamentals and applications of electrophoretic deposition (EPD). *Prog. Mater. Sci.* **2007**, *52*, 1−61.

(17) Holgado, M.; García-Santamaría, F.; Blanco, A.; Ibisate, M.; Cintas, A.; Míguez, H.; Serna, C. J.; Molpeceres, C.; Requena, J.; Mifsud, A.; Meseguer, F.; López, C. Electrophoretic Deposition To Control Artificial Opal Growth. *Langmuir* **1999**, *15*, 4701−4704.

(18) Rogach, A. L.; Kotov, N. A.; Koktysh, D. S.; Ostrander, J. W.; Ragoisha, G. A. Electrophoretic Deposition of Latex-Based 3D Colloidal Photonic Crystals: A Technique for Rapid Production of High-Quality Opals. *Chem. Mater.* **2000**, *12*, 2721−2726.

(19) Park, J. S.; Saintillan, D. Direct Numerical Simulations of Electrophoretic Deposition of Charged Colloidal Suspensions. *Key Eng. Mater.* **2012**, *507*, 47−51.

(20) Huang, Y.-J.; Lai, C.-H.; Wu, P.-W. Fabrication of Large-Area Colloidal Crystals by Electrophoretic Deposition in Vertical Arrangement. *Electrochem. Solid-State Lett.* **2008**, *11*, P20−P22.

(21) Katagiri, K.; Tanaka, Y.; Uemura, K.; Inumaru, K.; Seki, T.; Takeoka, Y. Structural Color Coating Films Composed of an Amorphous Array of Colloidal Particles via Electrophoretic Deposition. *NPG Asia Mater.* **2017**, *9*, No. e355.

(22) Napolskii, K. S.; Sapoletova, N. A.; Gorozhankin, D. F.; Eliseev, A. A.; Chernyshov, D. Y.; Byelov, D. V.; Grigoryeva, N. A.; Mistonov, A. A.; Bouwman, W. G.; Kvashnina, K. O.; Lukashin, A. V.; Snigirev, A. A.; Vassilieva, A. V.; Grigoriev, S. V.; Petukhov, A. V. Fabrication of Artificial Opals by Electric-Field-Assisted Vertical Deposition. *Langmuir* **2010**, *26*, 2346−2351.

(23) Muldarisnur, M.; Marlow, F. Opal Films Made by the Capillary Deposition Method: Crystal Orientation and Defects. *J. Phys. Chem. C* **2011**, *115*, 414−418.

(24) Muldarisnur, M.; Marlow, F. Spectroscopic Investigation of Opal Formation from Suspensions. *J. Phys. Chem. C* **2017**, *121*, 18274−18279.

(25) Muldarisnur, M.; Marlow, F. Observation of Nano-Dewetting in Colloidal Crystal Drying. *Angew. Chem., Int. Ed.* **2014**, *53*, 8761−8764.

(26) Basu, R. N.; Randall, C. A.; Mayo, M. J. Fabrication of Dense Zirconia Electrolyte Films for Tubular Solid Oxide Fuel Cells by Electrophoretic Deposition. *J. Am. Ceram. Soc.* **2001**, *84*, 33−40.

(27) Muldarisnur, M.; Popa, I.; Marlow, F. Angle-resolved transmission spectroscopy of opal films. *Phys. Rev. B: Condens. Matter Mater. Phys.* **2012**, *86*, 024105.

(28) Hartsuiker, A.; Vos, W. L. Structural Properties of Opals Grown with Vertical Controlled Drying. *Langmuir* **2008**, *24*, 4670−4675.

(29) Bertone, J. F.; Jiang, P.; Hwang, K. S.; Mittleman, D. M.; Colvin, V. L. Thickness Dependence of the Optical Properties of Ordered Silica-Air and Air-Polymer Photonic Crystals. *Phys. Rev. Lett.* **1999**, *83*, 300−303.

(30) Popa, I.; Marlow, F. Post-deposition opal evolution. *ChemPhysChem* **2008**, *9*, 1541−1547.

(31) Lee, W. P.; Routh, A. F. Why Do Drying Films Crack? *Langmuir* **2004**, *20*, 9885−9888.

(32) Suh, Y.; Pham, Q.; Shao, B.; Won, Y. The Control of Colloidal Grain Boundaries through Evaporative Vertical Self-Assembly. *Small* **2019**, *15*, 1804523.

(33) Sapoletova, N. A.; Martynova, N. A.; Napolskii, K. S.; Eliseev, A. A.; Lukashin, A. V.; Kolesnik, I. V.; Petukhov, D. I.; Kushnir, S. E.; Vassilieva, A. V.; Grigoriev, S. V.; Grigoryeva, N. A.; Mistonov, A. A.; Byelov, D. V.; Tret'yakov, Y. D. Electric-field-assisted self-assembly of colloidal particles. *Phys. Solid State* **2011**, *53*, 1126−1130.